Applied Catalysis B: Environmental 313 (2022) 121468

Contents lists available at ScienceDirect

Applied Catalysis B: Environmental

journal homepage: www.elsevier.com/locate/apcatb

Synergistic effect of Cu^+ single atoms and Cu nanoparticles supported on alumina boosting water-gas shift reaction

Zhonghui Cui [a,b], Song Song [a,*], Huibin Liu [a,b], Yingtian Zhang [a,b], Fei Gao [c], Tong Ding [a], Ye Tian [a], Xiaobin Fan [a,b], Xingang Li [a,b,d,**]

[a] State Key Laboratory of Chemical Engineering, Tianjin Key Laboratory of Applied Catalysis Science and Engineering, School of Chemical Engineering and Technology, Institute of Shaoxing, Tianjin University, Tianjin 300350, PR China
[b] Chemistry and Chemical Engineering Guangdong Laboratory, Shantou 515031, PR China
[c] Jiangsu Key Laboratory of Vehicle Emissions Control, Lab of XPS, Center of Modern Analysis, School of Environment, Nanjing University, Nanjing 210093, PR China
[d] School of Chemistry and Chemical Engineering, Lanzhou Jiaotong University, Lanzhou 730070, PR China

ARTICLE INFO

Keywords:
Single atom catalysts
Supported metal catalysts
Synergistic effect
Copper
Water-gas shift reaction

ABSTRACT

The water-gas shift reaction (WGSR) is an important industrial process for H_2 production. Here, we rationally construct alumina supported dual-site copper catalysts, i.e. Cu^+ single atoms (Cu_1^+) surrounding Cu nanoparticles (Cu_{NP}^0), for WGSR. Our findings show that CO is tightly adsorbed on surface-enriched Cu_1^+ sites to inhibit competitive adsorption with H_2O on Cu_{NP}^0 sites. The number of adsorbed CO is two orders of magnitude higher than that on conventional Cu-based catalysts. It significantly increases surface CO concentration, and forms a unique structure of Cu_{NP}^0 "islands" immerged in CO "pool". Benefiting from synergy of Cu_1^+ and Cu_{NP}^0 sites, the catalyst with 12% Cu loading exhibits extraordinary and robust catalytic activity, compared to benchmark Cu-Zn-Al catalyst, especially at low temperatures, e.g. 200 °C. The catalyst design strategy and facile synthesis methodology employed in this work could be potentially applied in other related industrial reactions.

1. Introduction

Supported metal catalysts have been applied to many industrial processes, e.g. Cu-Zn-Al catalyst for water-gas shift reaction (WGSR) [1–3]. In recent decades, the application of nanotechnology in heterogeneous catalysis promotes the rapid development of such catalysts from nanoparticles to single atoms [4,5]. Single atom catalysts (SACs) could maximize metal utilization and often show specific catalytic performance [6,7]. However, SACs have their own limitations compared to metal nanoparticles (NPs) catalysts. For example, oxidative valence of SACs restricts applications requiring zero-valent metal sites [8]. Encouragingly, recent studies show that simultaneously constructing single atoms and metal NPs on catalysts is a possible way to overcome these disadvantages [9,10].

WGSR is of great significance for H_2 production industry with Cu catalysts, e.g. Cu-Zn-Al, for decades [11]. Generally, metallic Cu NPs (Cu_{NP}^0) or their interfaces with support are active sites for CO adsorption/activation, and H_2O adsorption/dissociation [12,13]. Nevertheless, the disadvantages of weak CO adsorption and competitive adsorption of CO and H_2O on Cu_{NP}^0 make them suffer from low activity [14,15]. Recently, studies show that CO adsorption on single atoms is much stronger than that on metal NPs [16]. Therefore, it is meaningful to introduce Cu^+ single atoms (Cu_1^+) into Cu catalysts to prevent competitive adsorption of CO on Cu_{NP}^0 with H_2O by enhancing CO adsorption on Cu_1^+.

Herein, we design catalysts containing Cu_1^+ and Cu_{NP}^0 dual-sites, and elucidate their synergistic roles in WGSR via in situ experiments and density functional theory (DFT) calculations. The catalyst precursor (Cu_1^{2+}/Al_2O_3) with the target structure of Cu^{2+} single atoms (Cu_1^{2+}) is synthesized with sol-gel method. Then, Cu_1^{2+} species are transformed to Cu_1^+ and Cu_{NP}^0 sites by reduction. Mechanistic studies demonstrate that Cu_1^+ sites not only strongly adsorb CO and act as CO "pool" to increase CO concentration surrounding Cu_{NP}^0 sites, but also inhibit competitive adsorption of CO on Cu_{NP}^0, inducing significantly improved WGSR performance. Rational development of such Cu catalysts with synergistic single atoms and metal NPs provides a promising strategy to explore

* Corresponding author.
** Corresponding author at: State Key Laboratory of Chemical Engineering, Tianjin Key Laboratory of Applied Catalysis Science and Engineering, School of Chemical Engineering and Technology, Institute of Shaoxing, Tianjin University, Tianjin 300350, PR China.
E-mail addresses: ssong@tju.edu.cn (S. Song), xingang_li@tju.edu.cn (X. Li).

https://doi.org/10.1016/j.apcatb.2022.121468
Received 5 February 2022; Received in revised form 18 April 2022; Accepted 29 April 2022
Available online 3 May 2022

other similar catalyst systems.

2. Experimental

2.1. Sample preparation

Synthesis of Cu_1^{2+}/Al_2O_3 samples. Cu_1^{2+}/Al_2O_3 samples were prepared by sol-gel method according to previous reports [17,18]. Typically, a certain amount of $Cu(NO_3)_2$•3 H_2O was dissolved with the 0.8–1.0 g of Pluronic P123 in 20 ml of anhydrous ethanol at room temperature. Then 1.4–1.6 ml of 67 wt% nitric acid and a certain amount of aluminum iso-propoxide were added to the above solution with vigorous stirring. The mixture is continued stirring at room temperature for 8 h. The blue precipitate was dried at 60 °C for 48 h and then calcined at 500 °C for 6 h. The total quantity of metal species (10 mmol, aluminum and copper) was kept constant, and the mass ratio of copper to the whole sample was adjusted accordingly (0%, 4%,12%, and 20%). The final calcined samples were denoted as x Cu_1^{2+}/Al_2O_3, where x (x = 4%, 12% and 20%) represents the mass ratio as described above.

Synthesis of $Cu_1^{+}+Cu_{NP}^{0}/Al_2O_3$ samples. $Cu_1^{+}+Cu_{NP}^{0}/Al_2O_3$ samples were prepared by reducing the Cu_1^{2+}/Al_2O_3 samples in the 10% H_2/N_2 flow (30 ml min^{-1}) at 400 °C for 1 h. The final reduced samples were denoted as x $Cu_1^{+}+Cu_{NP}^{0}/Al_2O_3$, where x (x = 4%, 12% and 20%) represents the mass ratio as described above.

Synthesis of Cu/Al_2O_3-IM sample. For comparison, the Cu/Al_2O_3-IM sample containing 12 wt% of Cu was prepared by wet impregnation method using rotary evaporators with an aqueous solution of Cu $(NO_3)_2$•3 H_2O on Al_2O_3 (prepared by sol-gel). The conditions of drying and calcinations were the same as the x Cu_1^{2+}/Al_2O_3 samples, and denoted as12% CuO/Al_2O_3-IM. After reduction by H_2, the sample was denoted as 12% Cu/Al_2O_3-IM.

Synthesis of Cu-Zn-Al sample. Cu-Zn-Al was synthesized by co-precipitation method according to previous reports [19]. The mass ratio of CuO, ZnO and Al_2O_3 in the sample were 63 wt%, 27 wt% and 10 wt%, respectively.

2.2. Characterization techniques

The X-ray diffraction patterns were collected on a Bruker D8 diffractometer, employing the Cu Kα radiation (λ = 0.15418 nm). Transmission electron microscopy (TEM) and EDX elemental maps were carried out on a JEOL JEM-2800 system. HAADF-STEM image was obtained on a Titan ETEM G2 80–300 (FEI, American) equipped with spherical aberration correctors. X-ray photoelectron spectroscopy (XPS) analysis was performed on an ESCALAB 250 high performance electron spectrometer using monochromatized Al Kα (hν = 1486.7 eV) as the radiation source. The structural properties of the catalysts were acquired by a N_2 adsorption-desorption technique on a Quantachrome QuadraSorb SI instrument at 77 K. The copper dispersion and the metallic Cu surface areas were obtained by N_2O (2% N_2O/N_2, 30 ml min^{-1}) titration using XianQuan TP-5080 instrument. X-ray Absorption Fine Structure (XAFS) was performed at beamline 1W1B of Beijing Synchrotron Radiation Facility (BSRF) and BL14W1 of Shanghai Synchrotron Radiation Facility (SSRF). CuO, Cu_2O and Cu foil were selected as references. The spectrum was analyzed by the software of Athena. The in situ Diffuse Reflectance Infrared Fourier Transform Spectroscopy (DRIFTS) experiment was performed at the Harrick HVC high temperature transmission cell in the range of 400–4000 cm^{-1} [20]. The details were described in Supporting Information materials.

In situ XPS measurements upon reduction without exposure to air were performed as previous reports [11]. The x Cu_1^{2+}/Al_2O_3 samples were heated to 400 °C at a rate of 10 °C min^{-1} and kept for 1 h in 5% H_2/N_2 (flow rate: 30 ml min^{-1}) to acquire x $Cu_1^{+}+Cu_{NP}^{0}/Al_2O_3$ catalysts.

2.3. Catalytic evaluations

Catalytic measurement was conducted in a continuous flow fixed-bed with a quartz reactor. Before reaction, all of the samples were reduced in 10% H_2/N_2 flow at 400 °C for 1 h. The reactant consisting of 10% H_2O (g) and 5% CO was at constant weight hourly space velocity (WHSV) of 18000 ml g_{cat}^{-1} h^{-1}, with N_2 as the balanced gas. The composition of the gas was detected by an online gas Chromatograph (Agilent 7890A). The CO conversion was calculated as follows:

$$X_{CO}=(F_{(CO,in)}-F_{(CO,out)})\ /F_{(CO,in)}\ \times 100\% \quad (1)$$

Where $F_{(CO,in)}$ is the influent molar flow rate of CO; $F_{(CO,out)}$ is the effluent molar flow rate of CO; X_{CO} is CO conversion.

The kinetics evaluations were conducted in the same continuous flow fixed-bed with a quartz reactor as described previously. The internal and external diffusion limitations were eliminated. The reactant consisting of 10% H_2O (g) and 5% CO was at constant weight hourly space velocity (WHSV) of 54000 ml g_{cat}^{-1} h^{-1}, with 85% N_2 as the balanced gas. The measurement was conducted within temperature range from 100 °C to 250 °C, where the CO conversion was below 10%. The reaction rate (r) was calculated as follows:

$$r = (X_{co} \times F_{(co,in)}) / W_{cat} \quad (2)$$

The value of turnover frequency (TOF) was calculated as follows:

$$TOF = (F_{CO} \times X_{CO}) / (W_{cat} \times n_{sites}) \quad (3)$$

Where W_{cat} is the weight of the loaded catalyst; n_{site} is the number of surface active sites in mole.

The apparent activation energy (E_a) of the catalysts was determined by plotting the Arrhenius as follows:

$$k = A\ e^{(-Ea/RT)} \quad (4)$$

The stability evaluation of the catalyst was conducted under the same reaction conditions as the catalytic measurement. After pre-reduction, the catalyst was exposed to the reaction gas at 225 °C with a WHSV of 18000 ml g_{cat}^{-1} h^{-1}.

2.4. Computational method

The calculations were executed by density functional theory (DFT) with the Vienna ab-initio simulation package (VASP) [21]. Here we chose the projector augmented wave (PAW) method [22] and Perdew-Burke-Ernzerhof functional [23] to describe the coactions between ion cores and valence electrons were described by the projector augmented wave (PAW) method and calculated the exchange and correlation energies, respectively. The wave functions at each k-point were expanded with a plane wave basis set. The cutoff energy was set to 520 eV. The structures of the whole calculations were optimized using a force-based conjugate-gradient method until the energy was converged to 1.0×10^{-5} eV/atom and the force to 0.02 eV/Å, while the Brillouin zone was conducted using a 1 × 1 × 1 Monkhorst-Pack grid.

We adopted a periodic single layer of α-Al_2O_3 (001) slab model to substitute amorphous alumina [24]. The Cu_{NP}^{0}/Al_2O_3 model was constructed of the Cu (001) layer and the α-Al_2O_3 (001) slab, while the Cu_2O (111) layer was selected for Cu_{NP}^{+}/Al_2O_3 model. A single Cu atom was anchored on the surface of the slab for Cu_1^{+}/Al_2O_3. To shield periodic interaction, a 20 Å thick vacuum layer was added along the c direction.

3. Result and discussion

3.1. Structure properties

The dual-site Cu catalysts were prepared by sol-gel method [17,18]. Briefly, the xerogel precursors were synthesized via evaporation-induced self-assembling of ethanol solution containing

Cu^{2+}, Al^{3+}, and P123. After calcination, the catalyst precursors of Cu_1^{2+}/Al_2O_3 are obtained, in which Cu species are highly dispersed Cu^{2+} single atoms. In addition, the as-prepared Al_2O_3 support would contain a certain amount of penta-coordinated Al^{3+} (Al^{3+}_{penta}) according to previous works [25], which could strongly and stably anchor single atoms [26]. During the reduction process, some Cu_1^{2+} species were easily transformed to Cu^0_{NP} species after reduction due to their weak interaction with support, while other Cu_1^{2+} species could only be reduced to Cu_1^+ species resulting from their strong interaction with Al^{3+}_{penta}. Thereafter, the catalysts of Cu_1^++Cu^0_{NP}/Al_2O_3 are achieved through reduction of Cu_1^{2+}/Al_2O_3.

N_2 adsorption-desorption isotherms and X-ray diffraction (XRD) patterns of the as-synthesized samples confirm the mesoporous nature and the amorphous structure of Al_2O_3 support prepared by sol-gel method in Figs. S1–S2, and Table S1. CuO phase is not detected in the XRD patterns of Cu_1^{2+}/Al_2O_3, while two obvious peaks (~ 43.5 and 50.4°) assigning to metallic Cu phase appear in those of Cu_1^++Cu^0_{NP}/Al_2O_3 in Fig. S2 [20]. The transmission electron microscopy (TEM) images of the as-synthesized samples were shown in Fig. 1A, B. CuO NPs are not observed on 12% Cu_1^{2+}/Al_2O_3, resulting from their highly uniform dispersion on Al_2O_3 (Fig. 1A). After reduction in H_2 at 400 °C, Cu NPs appear in 12% Cu_1^++Cu^0_{NP}/Al_2O_3 with spacing lattice fringe of ~0.208 nm for cubic Cu (111) plane (Fig. 1B) [27]. In addition, the average size of Cu NPs is in accordance with the XRD results in Fig. S2 and Table S2. The energy dispersive X-ray (EDX) mappings of 12% Cu_1^++Cu^0_{NP}/Al_2O_3 highlight the existence of Cu NPs and show the uniform dispersion of Cu, Al, and O elements (Fig. 1C). In Fig. 1D, the aberration-corrected high angle annular dark field (AC-HAADF) scanning transmission electron microscopy (STEM) image shows the coexistence of Cu single atoms (red circle highlighted) and Cu NP (yellow broken circle highlighted), and especially, the latter is tightly surrounded by the formers.

3.2. Chemical states

X-ray absorption technique was utilized to illustrate electronic structure and local coordination environment of Cu species in Cu_1^++Cu^0_{NP}/Al_2O_3. The normalized Cu K-edge X-ray absorption near edge structure (XANES) spectra of Cu_1^{2+}/Al_2O_3 in Fig. S3A suggest that Cu species mainly exist as CuO. In Figs. S3B, S4 and Table S3, radial structure function (RSF) curves display the main peak at ~ 1.5 Å, assigning to the first Cu–O shell for CuO [28,29], and no peak belonging to the Cu–Cu coordination was detected, demonstrating that Cu species exist as Cu^{2+} single atoms. For Cu_1^++Cu^0_{NP}/Al_2O_3, the XANES spectra display a slightly stronger white-line at ~ 8980 eV relative to Cu_2O (Fig. 2A) [30]. The RSF curves in Fig. 2B, S5 and Table S4 exhibit two major peaks at ~ 1.5 and 2.1 Å, assigning to the first Cu–O shell for Cu_2O and Cu–Cu shell for metallic Cu, respectively [31]. No Cu–Cu shell for Cu_2O is detected in all Cu_1^++Cu^0_{NP}/Al_2O_3 samples, indicating that Cu^+ species exist as single atoms [32]. Therefore, the results of XAFS and STEM in Fig. 1-2 confirm the coexistence of Cu_1^+ and Cu^0_{NP} sites on the as-synthesized samples.

In situ X-ray photoelectron spectroscopy (XPS) was further performed to investigate chemical states of copper species on Cu_1^++Cu^0_{NP}/

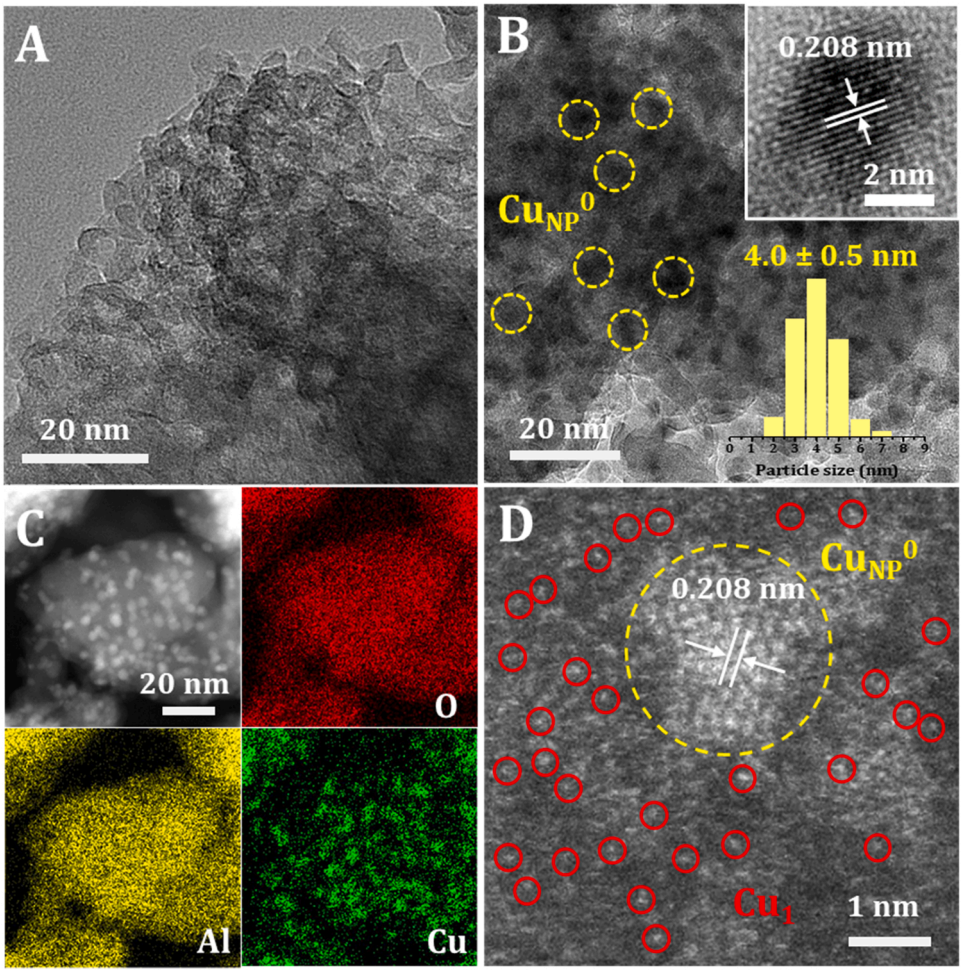

Fig. 1. A) TEM image of 12% Cu_1^{2+}/Al_2O_3. B) TEM and HRTEM images, C) dark-field STEM image and EDX mapping, and D) AC-HAADF-STEM image of 12% Cu_1^++Cu^0_{NP}/Al_2O_3.

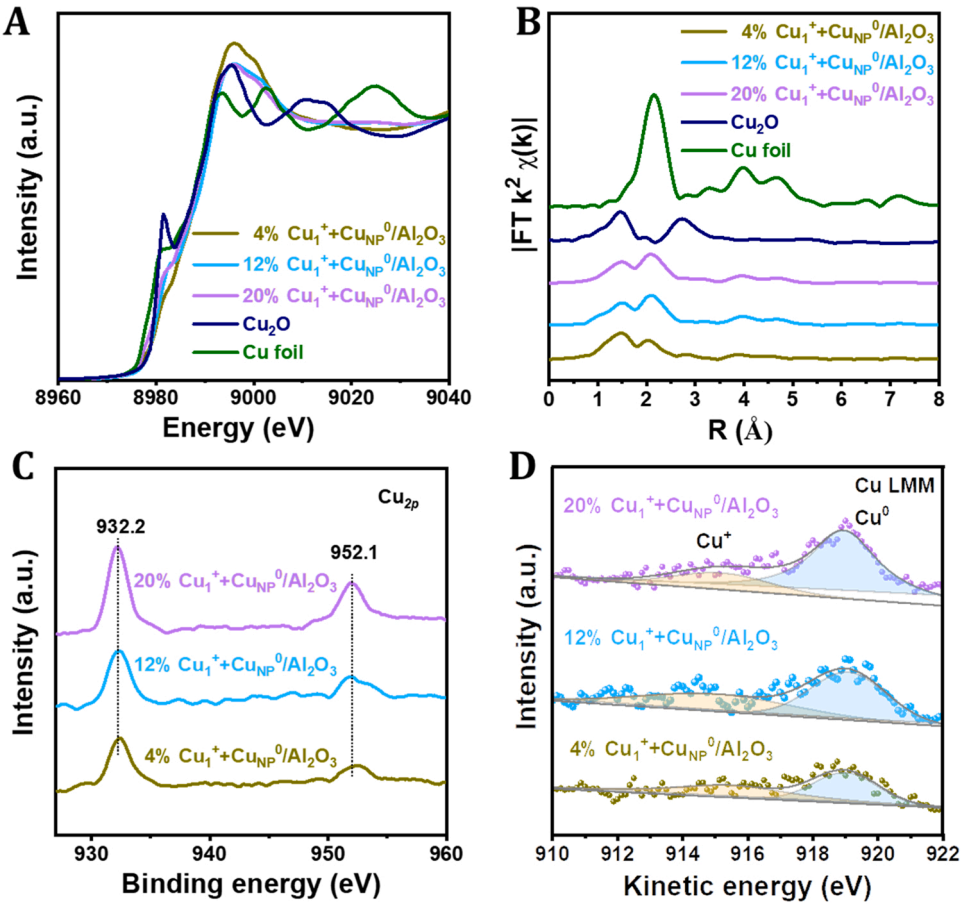

Fig. 2. A) Normalized Cu K-edge XANES spectra. B) Radial structure function (RSF) curves. C) In situ Cu 2*p* XPS spectra and D) In situ Cu LMM Auger spectra of Cu_1^++Cu_{NP}^0/Al_2O_3.

Al_2O_3 in Fig. 2C. These spectra exhibit two peaks at ~ 932.2 eV (Cu $2p_{3/2}$) and ~ 952.1 eV (Cu $2p_{1/2}$), assigning to Cu^+ and/ or Cu^0 states [33]. In situ Cu LMM Auger electron spectroscopy (AES) spectra demonstrate the presence of both species rather than Cu^{2+}, and the value of Cu^0/Cu^+ ratio gradually increases from 1.0 to 4.5 with increasing Cu loadings from 4% to 20% (Table S5). Additionally, the as-synthesized samples show higher reducibility than the conventional supported one (Fig. S6).

3.3. Catalytic performances

The catalytic performance of the catalysts in the temperature range of 100–300 ℃ was shown in Fig. 3. 12% Cu_1^++Cu_{NP}^0/Al_2O_3 presented the highest activity, and achieved 90% CO conversion even at the low temperature of 200 °C. But, 12% Cu/Al_2O_3-IM, prepared with impregnation method, gave the lowest activity. Here, the turnover frequency (TOF) value of 12% Cu_1^++Cu_{NP}^0/Al_2O_3 was also the highest in Table S6. Cu-Zn-Al, a well-known Cu catalyst in WGSR, exhibited a moderate activity with 85% CO conversion at 300 °C. However, only 30% CO conversion at 200 °C was attained, which is much lower than that of 12% Cu_1^++Cu_{NP}^0/Al_2O_3. Interestingly, all selected Cu-based catalysts exhibited the similar apparent activation energy, which were close to most of reported supported Cu catalysts [34]. We believe that they obey the similar reaction mechanism. Since Cu_{NP}^0 sites play a key role in WGSR over Cu-Zn-Al [35], the high activity of 12% Cu_1^++Cu_{NP}^0/Al_2O_3 should be due to the coexistence of Cu_1^+ and Cu_{NP}^0 dual-sites.

In addition, 12% Cu_1^++Cu_{NP}^0/Al_2O_3 maintained a relatively stable catalytic performance at 225 °C during the test up to 100 h, which is comparable to that of Cu-Zn-Al catalyst (Fig. 3C). The AC-HAAD-STEM image of spent 12% Cu_1^++Cu_{NP}^0/Al_2O_3 demonstrates the coexistence of Cu single atoms (red circle highlighted) and Cu NP (yellow broken circle highlighted) after the long-term reaction, as shown in Fig. S7. From an application point of view, the catalyst involved in fuel cell vehicles need satisfy start-stop cycles of engines [36,37]. For cyclic start-stop tests, the reaction temperature raised to 225 °C and hold for 1 h for catalytic evaluation, and then cooled down to 25 °C and maintained for 1 h. In Fig. 3D, CO conversion over 12% Cu_1^++Cu_{NP}^0/Al_2O_3 slightly dropped after eight cycles. It demonstrates that the sample exhibits high activity and stability for WGSR, especially at low operating temperatures. Importantly, the robust nature in the start-stop cycle tests demonstrates its potential industrial applications.

3.4. Reaction mechanisms

The diffuse reflectance infrared fourier transform spectroscopy (DRIFTS) spectra of CO adsorption on the samples were shown in Fig. 4A. A vibrational band at ~ 2105 cm^{-1} is observed on all of the samples, assigning to CO linearly adsorbed on Cu^+ species [38]. Strikingly, by integrating the band area, the number of adsorbed CO on 12% Cu_1^++Cu_{NP}^0/Al_2O_3 is qualitative two orders of magnitude higher than that on 12% Cu/Al_2O_3-IM and Cu-Zn-Al. In addition, the redshift of CO adsorption band on 12% Cu_1^++Cu_{NP}^0/Al_2O_3 indicates its stronger CO adsorption ability [39]. The DFT calculations were further conducted to study CO adsorption on different kinds of Cu sites. Three models, including Cu NPs (Cu_{NP}^0/Al_2O_3), Cu_2O NPs (Cu_{NP}^+/Al_2O_3), and Cu^+ single atoms (Cu_1^+/Al_2O_3), were constructed and optimized (Fig. S8). The computational details of our calculations were illustrated in Supporting Information. In Fig. 4B, the adsorption energy of CO on Cu_{NP}^0/Al_2O_3, Cu_{NP}^+/Al_2O_3, and Cu_1^+/Al_2O_3 is −0.28, −0.33, and −0.74 eV,

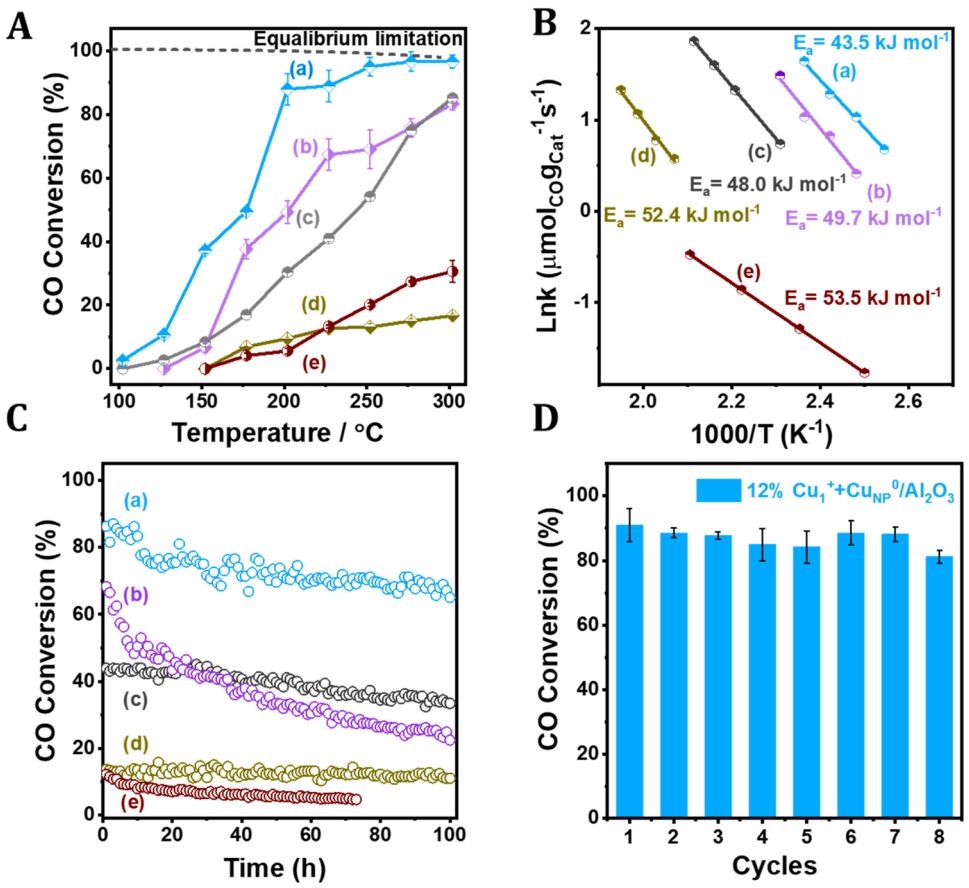

Fig. 3. A) Catalytic performance, B) Arrhenius plots and C) stability tests of the catalysts: (a) 12% Cu_1^++Cu_{NP}^0/Al_2O_3, (b) 20% Cu_1^++Cu_{NP}^0/Al_2O_3, (c) Cu-Zn-Al, (d) 4% Cu_1^++Cu_{NP}^0/Al_2O_3, (e) 12% Cu/Al_2O_3-IM. D) Start-stop cycle tests of 12% Cu_1^++Cu_{NP}^0/Al_2O_3. Reaction conditions: WHSV= 18000 ml g_{cat}^{-1} h^{-1}, 5% CO/10% H_2O/N_2 balance, T = 225 °C for (C, D).

respectively, suggesting that Cu_1^+ sites bind CO molecule more strongly than others, which is in agreement with the in situ DRIFTS results in Fig. 4A.

In situ DRIFTS spectra (Fig. 4C) of CO adsorption on the prehydroxylated samples display the characteristic vibrational bands of carboxyl species, including bidentate carbonate and bicarbonate species (1607 and 1423 cm^{-1}) [40]. Thus, WGSR on the samples mainly follows the associative mechanism with carboxyl species as intermediates [41]. It coincides with the results in Fig. 3B that 12% Cu_1^++Cu_{NP}^0/Al_2O_3 and Cu-Zn-Al had the similar activation energy values. Here, the band intensity of carbonate species on 12% Cu_1^++Cu_{NP}^0/Al_2O_3 is much stronger than that on other samples, demonstrating that more intermediates are formed, coinciding with the former's higher activity (Fig. 3A). Generally, H_2O molecules adsorb and dissociate on Cu_{NP}^0 sites during WGSR [42]. In Fig. 1D, surface-enriched Cu^+ single atoms with stronger CO adsorbability (Fig. 4A) tightly surround Cu NPs. This unique structure of Cu_1^++Cu_{NP}^0/Al_2O_3 will inevitably inhibit CO competitive adsorption on Cu_{NP}^0 sites with H_2O. All of these merits dramatically boost WGSR even at low operating temperatures (e.g. 200 °C).

In addition, 12% Cu_1^++Cu_{NP}^0/Al_2O_3 was reduced in H_2 at different temperatures (300 °C, 400 °C, and 500 °C) to study the effect of metal-support interaction. The XRD results show that these catalysts had the similar particle size of metallic Cu NPs (~ 3.7 nm) in Fig. S9 and Table S7. The DRIFTS study of CO adsorption on 12% Cu_1^++Cu_{NP}^0/Al_2O_3 displays that the intensity of IR band assigning to CO linearly adsorbed on Cu^+ decreased with an increase of reduction temperatures, indicating that 12% Cu_1^++Cu_{NP}^0/Al_2O_3-500 possessed less Cu_1^+ sites and more Cu_{NP}^0 sites (Fig. 4D). Considering their similar particle size, 12% Cu_1^++Cu_{NP}^0/Al_2O_3-500 with more Cu_{NP}^0 sites should exhibit more pronounced effect of metal-support interactions than others, while the catalytic activity of 12% Cu_1^++Cu_{NP}^0/Al_2O_3-400 was the highest in Fig. 4E. The results in Figs. 4D, E, S9, and Table S7 demonstrate that the excellent activity of 12% Cu_1^++Cu_{NP}^0/Al_2O_3 is mainly attributed to synergistic effect of Cu_1^+ and Cu_{NP}^0 rather than the effect of metal-support interaction. As a conclusion, the synergistic effect of Cu_1^+ and Cu_{NP}^0 dual-sites is illustrated in Fig. 4F. Cu_1^+ sites strongly bind CO molecules, and increase CO concentration on catalyst surface to form a CO "pool". Cu_{NP}^0 sites are still the main catalytic active sites for WGSR like other supported Cu catalysts. The role of Cu_1^+ sites not only provide CO "pool" to increase CO concentration around Cu_{NP}^0 sites (island), but also inhibits competitive adsorption of CO on Cu_{NP}^0 sites with H_2O, thereby enhancing the catalytic performance.

4. Conclusion

In summary, we develop the alumina supported copper catalysts containing dual-sites of Cu_1^+ and Cu_{NP}^0. 12% Cu_1^++Cu_{NP}^0/Al_2O_3 exhibits the outstanding WGSR activity compared to the conventional benchmark Cu-Zn-Al catalyst, especially at low operating temperatures like 200 °C, due to the synergistic effect of the dual-sites. Its robust nature in the start-stop cycles and long-term stability tests implies promising potential for industrial applications. This work opens a new avenue for rational design of robust metal catalysts with synergy of single atoms and nanoparticles for other related industrial processes.

CRediT authorship contribution statement

Xingang Li and **Song Song** conceived and supervised the project.

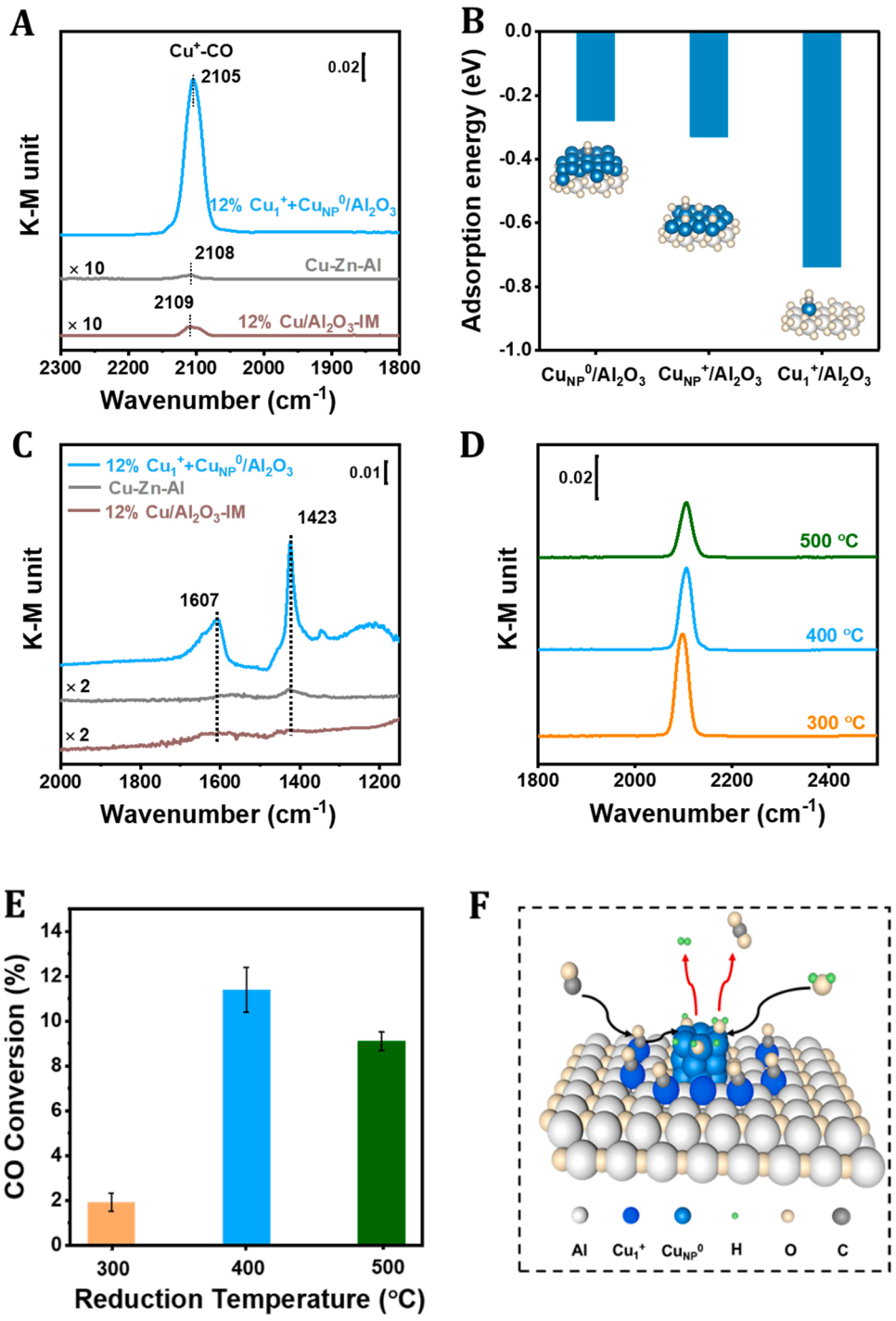

Fig. 4. A) In situ DRIFTS spectra of CO adsorption at 25 °C. B) Adsorption energy of CO on Cu^0_{NP}/Al_2O_3, Cu^+_{NP}/Al_2O_3, and Cu^+_1/Al_2O_3. C) In situ DRIFTS spectra of CO adsorption at 200 °C after exposing to H_2O atmosphere at 200 °C for 30 min. D) in situ DRIFTS spectra of CO adsorption, and E) WGSR activity of 12% $Cu^+ + Cu^0_{NP}/Al_2O_3$ at different reduction temperatures (300 °C, 400 °C, 500 °C). Reaction conditions: T = 125 °C, WHSV= 18000 ml g^{-1}_{cat} h^{-1}. F) Schematic illustration of the reaction mechanism.

Zhonghui Cui conducted experiments and analyzed data. Yingtian Zhang participated in some experiments. **Huibin Liu** and **Xiaobin Fan** performed DFT studies and analyzed the data. **Fei Gao** conduced in situ XPS characterizations and analyzed the data. **Tong Ding** and **Ye Tian** analyzed the data. **Xingang Li**, **Song Song**, and **Zhonghui Cui** wrote the paper. All authors discussed the results and edited the manuscript.

Declaration of Competing Interest

The authors declare that they have no known competing financial interests or personal relationships that could have appeared to influence the work reported in this paper.

Acknowledgements

The authors thank the financial support from National Natural Science Foundation of China (Grant No. 22102113), the Chemistry and Chemical Engineering Guangdong Laboratory (Grant No. 1912011), and State Key Laboratory of Chemical Engineering (SKL-ChE-20B01). We thank Dr. Z. Jiang from 14W1 station of Shanghai Synchrotron Radiation Facility and Dr. J. Zhang from 1W1B station of Beijing Synchrotron Radiation Facility for XAFS tests. We would like to thank Dr. L. Di from School of Materials Science and Engineering, Nankai University for TEM (JEM-2800) tests.

Appendix A. Supporting information

Supplementary data associated with this article can be found in the online version at doi:10.1016/j.apcatb.2022.121468.

References

[1] M. Behrens, F. Studt, I. Kasatkin, S. Kühl, M. Hävecker, F. Abild-Pedersen, S. Zander, F. Girgsdies, P. Kurr, B.L. Kniep, M. Tovar, R.W. Fischer, J.K. Nørskov, R. Schlögl, The active site of methanol synthesis over $Cu/ZnO/Al_2O_3$ industrial catalysts, Science 336 (2012) 893–897, https://doi.org/10.1126/science.1219831.

[2] J.A. Rodriguez, S. Ma, P. Liu, J. Hrbek, J. Evans, M. Pérez, Activity of CeO_x and TiO_x nanoparticles grown on Au(111) in the water-gas shift reaction, Science 318 (2007) 1757–1760, https://doi.org/10.1126/science.1150038.

[3] X. Zhang, M. Zhang, Y. Deng, M. Xu, L. Artiglia, W. Wen, R. Gao, B. Chen, S. Yao, X. Zhang, M. Peng, J. Yan, A. Li, Z. Jiang, X. Gao, S. Cao, C. Yang, A.J. Kropf, J. Shi, J. Xie, M. Bi, J.A. Bokhoven, Y.W. Li, X. Wen, M. Flytzani-Stephanopoulos, C. Shi, W. Zhou, D. Ma, A stable low-temperature H_2-production catalyst by crowding Pt on α-MoC, Nature 589 (2021) 396–401, https://doi.org/10.1038/s41586-020-03130-6.

[4] Y. Liu, J. Goebl, Y. Yin, Templated synthesis of nanostructured materials, Chem. Soc. Rev. 42 (2013) 2610–2653, https://doi.org/10.1039/c2cs35369e.

[5] Y. Wu, D. Wang, Y. Li, Nanocrystals from solutions: catalysts, Chem. Soc. Rev. 43 (2014) 2112–2124, https://doi.org/10.1039/C3CS60221D.

[6] B. Qiao, A. Wang, X. Yang, L.F. Allard, Z. Jiang, Y. Cui, J. Liu, J. Li, T. Zhang, Single-atom catalysis of CO oxidation using Pt/FeO_x, Nat. Chem. 3 (2011) 634–641, https://doi.org/10.1038/nchem.1095.

[7] S. Cao, M. Yang, A.O. Elnabawy, A. Trimpalis, S. Li, C. Wang, F. Göltl, Z. Chen, J. Liu, J. Shan, M. Li, T. Haas, K.W. Chapman, S. Lee, L.F. Allard, M. Mavrikakis, M. Flytzani-Stephanopoulos, Single-atom gold oxo-clusters prepared in alkaline solutions catalyse the heterogeneous methanol self-coupling reactions, Nat. Chem. 11 (2019) 1098–1105, https://doi.org/10.1038/s41557-019-0345-3.

[8] Z. Li, S. Ji, Y. Liu, X. Cao, S. Tian, Y. Chen, Z. Niu, Y. Li, Well-defined materials for heterogeneous catalysis: from nanoparticles to isolated single-atom sites, Chem. Rev. 120 (2020) 623–682, https://doi.org/10.1021/acs.chemrev.9b00311.

[9] X. Yang, Y. Wang, X. Wang, B. Mei, E. Luo, Y. Li, Q. Meng, Z. Jin, Z. Jiang, C. Liu, J. Ge, W. Xing, CO-tolerant PEMFC anodes enabled by synergistic catalysis between iridium single-atom sites and nanoparticles, Angew. Chem. Int. Ed. 60 (2021) 26177–26183, https://doi.org/10.1002/anie.202110900.

[10] L. Wang, E. Guan, J. Zhang, J. Yang, Y. Zhu, Y. Han, M. Yang, C. Cen, G. Fu, B. C. Gates, F.S. Xiao, Single-site catalyst promoters accelerate metal-catalyzed nitroarene hydrogenation, Nat. Commun. 9 (2018) 1362, https://doi.org/10.1038/s41467-018-03810-y.

[11] Z. Zhang, S.S. Wang, R. Song, T. Cao, L. Luo, X. Chen, Y. Gao, J. Lu, W.X. Li, W. Huang, The most active Cu facet for low-temperature water gas shift reaction, Nat. Commun. 8 (2017) 488, https://doi.org/10.1038/s41467-017-00620-6.

[12] A. Chen, X. Yu, Y. Zhou, S. Miao, Y. Li, S. Kuld, J. Sehested, J. Liu, T. Aoki, S. Hong, M.F. Camellone, S. Fabris, J. Ning, C. Jin, C. Yang, A. Nefedov, C. Wöll, Y. Wang, W. Shen, Structure of the catalytically active copper–ceria interfacial perimeter, Nat. Catal. 2 (2019) 334–341, https://doi.org/10.1038/s41929-019-0226-6.

[13] C.S. Chen, T.W. Lai, C.C. Chen, Effect of active sites for a water–gas shift reaction on Cu nanoparticles, J. Catal. 273 (2010) 18–28, https://doi.org/10.1016/j.jcat.2010.04.019.

[14] C. Rhodes, G.J. Hutchings, A.M. Ward, Water-gas shift reaction: finding the mechanistic boundary, Catal. Today 23 (1995) 43–58, https://doi.org/10.1016/0920-5861(94)00135-o.

[15] Z. Bian, W. Zhong, Y. Yu, B. Jiang, S. Kawi, Cu/SiO_2 derived from copper phyllosilicate for low-temperature water-gas shift reaction: Role of Cu^+ sites, Int. J. Hydrog. Energy 45 (2020) 27078–27088, https://doi.org/10.1016/j.ijhydene.2020.07.054.

[16] J. Hulva, M. Meier, R. Bliem, Z. Jakub, F. Kraushofer, M. Schmid, U. Diebold, C. Franchini, G.S. Parkinson, Unraveling CO adsorption on model single-atom catalysts, Science 371 (2021) 375–379, https://doi.org/10.1126/science.abe5757.

[17] S.M. Morris, P.F. Fulvio, M. Jaroniec, Ordered mesoporous alumina-supported metal oxides, J. Am. Chem. Soc. 130 (2008) 15210–15216, https://doi.org/10.1021/ja806429q.

[18] Q. Yuan, A.X. Yin, C. Luo, L.D. Sun, Y.W. Zhang, W.T. Duan, H.T. Liu, C.H. Yan, Facile synthesis for ordered mesoporous ã-aluminas with high thermal stability, J. Am. Chem. Soc. 130 (2008) 15210–15216, https://doi.org/10.1021/ja0764308.

[19] X. Wang, K. Ma, L. Guo, Y. Tian, Q. Cheng, X. Bai, J. Huang, T. Ding, X. Li, $Cu/ZnO/SiO_2$ catalyst synthesized by reduction of ZnO-modified copper phyllosilicate for dimethyl ether steam reforming, Appl. Catal. A 540 (2017) 37–46, https://doi.org/10.1016/j.apcata.2017.04.013.

[20] K. Ma, Y. Tian, Z.J. Zhao, Q. Cheng, T. Ding, J. Zhang, L. Zheng, Z. Jiang, T. Abe, N. Tsubaki, J. Gong, X. Li, Achieving efficient and robust catalytic reforming on dual-sites of Cu species, Chem. Sci. 10 (2019) 2578–2584, https://doi.org/10.1039/C9SC00015A.

[21] G. Kresse, J. Furthmuller, Efficient iterative schemes for ab initio total-energy calculations using a plane-wave basis set, Phys. Rev. B 54 (1996) 11169–11186, https://doi.org/10.1103/PhysRevB.54.11169.

[22] P.E. Blochl, Projector augmented-wave method, Phys. Rev. B 50 (1994) 17953–17978, https://doi.org/10.1103/physrevb.50.17953.

[23] J.P. Perdew, K. Burke, M. Ernzerhof, Generalized gradient approximation made simple, Phys. Rev. Lett. 77 (1996) 3865–3868, https://doi.org/10.1103/PhysRevLett.78.1396.

[24] Z. Yang, S. Zhang, H. Zhao, A. Li, L. Luo, L. Guo, Subnano-FeO_x clusters anchored in an ultrathin amorphous Al_2O_3 nanosheet for styrene epoxidation, ACS Catal. 11 (2021) 11542–11550, https://doi.org/10.1021/acscatal.1c01366.

[25] Q. Yu, T. Y, H. Chen, G. Fang, X. Pan, X. Bao, The effect of Al^{3+} coordination structure on the propane dehydrogenation activity of $Pt/Ga/Al_2O_3$ catalysts, J. Energy Chem. 41 (2020) 93–99, https://doi.org/10.1016/j.jechem.2019.04.027.

[26] J.H. Kwak, J. Hu, D. Mei, C.W. Yi, D.H. Kim, C.H.F. Peden, L.F. Allard, J. Szanyi, Coordinatively unsaturated Al^{3+} centers as binding sites for active catalyst phases of platinum on γ-Al_2O_3, Science 325 (2009) 1670–1673, https://doi.org/10.1126/science.1176745.

[27] L. Zhao, Y. Qi, L. Song, S. Ning, S. Ouyang, H. Xu, J. Ye, Solar-driven water–gas shift reaction over CuO_x/Al_2O_3 with 1.1% of light-to-energy storage, Angew. Chem. Int. Ed. 58 (2019) 7708–7712, https://doi.org/10.1002/ange.201902324.

[28] F. Huang, Y. Deng, Y. Chen, S.X. Cai, M. Peng, Z. Jia, J. Xie, D. Xiao, X. Wen, N. Wang, Z. Jiang, H. Liu, D. Ma, Anchoring Cu_1 species over nanodiamond-graphene for semi-hydrogenation of acetylene, Nat. Commun. 10 (2019) 4431, https://doi.org/10.1038/s41467-019-12460-7.

[29] X. Guo, M. Xu, M. She, Y. Zhu, T. Shi, Z. Chen, L. Peng, X. Guo, M. Lin, W. Ding, Morphology-reserved synthesis of discrete nanosheets of CuO@ SAPO-34 and pore mouth catalysis for one-pot oxidation of cyclohexane, Angew. Chem. Int. Ed. 59 (2020) 2606–2611, https://doi.org/10.1002/ange.201911749.

[30] X. Zhang, G. Cui, H. Feng, L. Chen, H. Wang, B. Wang, X. Zhang, L. Zheng, S. Hong, M. Wei, Platinum–copper single atom alloy catalysts with high performance towards glycerol hydrogenolysis, Nat. Commun. 10 (2019) 5812, https://doi.org/10.1038/s41467-019-13685-2.

[31] V.L. Sushkevich, M. Artsiusheuski, Zhang, D. Klose, G. Jeschke, J.A. van Bokhoven, Identification of kinetic and spectroscopic signatures of copper sites for direct oxidation of methane to methanol, Angew. Chem. Int. Ed. 60 (2021) 15944–15953, https://doi.org/10.1002/anie.202101628.

[32] A. Beniya, S. Higashi, Towards dense single-atom catalysts for future automotive applications, Nat. Catal. 2 (2019) 590–602, https://doi.org/10.1038/s41929-019-0282-y.

[33] D.A. Svintsitskiy, T.Y. Kardash, O.A. Stonkus, E.M. Slavinskaya, A.I. Stadnichenko, S.V. Koscheev, A.P. Chupakhin, A.I. Boronin, In situ XRD, XPS, TEM, and TPR study of highly active in CO oxidation CuO nanopowders, J. Phys. Chem. C 117 (2013) 14588–14599, https://doi.org/10.1021/jp403339r.

[34] H. Yan, C. Yang, W.P. Shao, L.H. Cai, W.W. Wang, Z. Jin, C.J. Jia, Construction of stabilized bulk-nano interfaces for highly promoted inverse CeO_2/Cu catalyst, Nat. Commun. 10 (2019) 3470, https://doi.org/10.1038/s41467-019-11407-2.

[35] C. Ratnasamy, J.P. Wagner, Water gas shift catalysis, Catal. Rev. Sci. Eng. 51 (2009) 325–440, https://doi.org/10.1080/01614940903048661.

[36] N. Liu, M. Xu, Y. Yang, S. Zhang, J. Zhang, W. Wang, L. Zheng, S. Hong, M. Wei, $Au^{\delta-}-O_v-Ti^{3+}$ interfacial site: catalytic active center toward low-temperature water gas shift reaction, ACS Catal. 9 (2019) 2707–2710, https://doi.org/10.1021/acscatal.8b04913.

[37] J.L. Santos, T.R. Reina, S. Ivanova, M.A. Centeno, J.A. Odriozola, Gold promoted $Cu/ZnO/Al_2O_3$ catalysts prepared from hydrotalcite precursors: advanced materials for the WGS reaction, Appl. Catal. B 201 (2017) 310–317, https://doi.org/10.1016/j.apcatb.2016.08.017.

[38] J. Gu, M. Jian, L. Huang, Z. Sun, A. Li, Y. Pan, J. Yang, W. Wen, W. Zhou, Y. Lin, H. J. Wang, X. Liu, L. Wang, X. Shi, X. Huang, L. Cao, S. Chen, X. Zheng, H. Pan, J. Zhu, S. Wei, W.X. Li, J. Lu, Synergizing metal-support interactions and spatial confinement boosts dynamics of atomic nickel for hydrogenations, Nat. Nanotechnol. 16 (2021) 1141–1149, https://doi.org/10.1038/s41565-021-00951-y.

[39] S. Shang, C. Yang, C. Wang, J. Qin, Y. Li, Q. Gu, J. Shang, Transition-metal-containing porphyrin metal-organic frameworks as δ-backbonding adsorbents for NO_2 removal, Angew. Chem. Int. Ed.. 59 (2020) 19680–19683, https://doi.org/10.1002/anie.202007054.

[40] N.C. Nelson, M.T. Nguyen, V.A. Glezakou, R. Rousseau, J. Szanyi, Carboxyl intermediate formation via an in situ-generated metastable active site during water-gas shift catalysis, Nat. Catal.. 2 (2019) 916–924, https://doi.org/10.1038/s41929-019-0343-2.

[41] A.A. Gokhale, J.A. Dumesic, M. Mavrikakis, On the mechanism of low-temperature water gas shift reaction on copper, J. Am. Chem. Soc. 130 (2008) 1402–1414, https://doi.org/10.1021/ja0768237.

[42] B. Eren, D. Zherebetskyy, L.L. Patera, C.H. Wu, H. Bluhm, C. Africh, L.W. Wang, G. A. Somorjai, M. Salmeron, Activation of Cu (111) surface by decomposition into nanoclusters driven by CO adsorption, Science 351 (2016) 475–478, https://doi.org/10.1126/science.aad8868.